American Mineralogist, Volume 81, pages 1438–1451, 1996

Unequilibrated eucrites and the equilibrated Juvinas eucrite: Pyroxene REE systematics and major, minor, and trace element zoning

Aurora Pun and James J. Papike

Institute of Meteoritics, Department of Earth and Planetary Sciences, University of New Mexico, Albuquerque, New Mexico 87131-1126, U.S.A.

Abstract

In unequilibrated eucrites, pyroxene is a sensitive recorder of variables that affect their crystallization histories. Therefore, major, minor, and trace element systematics of pyroxene were evaluated from several unequilibrated eucrites and an equilibrated eucrite, Juvinas, by EMP and SIMS techniques. The Cr, Al, and Ti zoning trends in pyroxene reflect its igneous crystallization history, including the sequence of crystallization of pyroxene and plagioclase. The primary substitutional couples in unequilibrated pyroxene among Cr, Al, and Ti are $^{[6]}Cr^{3+}$-$^{[4]}Al^{3+}$, $^{[6]}Al^{3+}$-$^{[4]}Al^{3+}$, and $^{[6]}Ti^{4+}$-$2^{[4]}Al^{3+}$, with the $^{[6]}Ti^{4+}$-$2^{[4]}Al^{3+}$ couple dominating over $^{[6]}Al^{3+}$-$^{[4]}Al^{3+}$ following the onset of plagioclase crystallization. Reequilibration erases the primary igneous zoning trends of Cr, Al, and Ti, and the dominant substitutional couples in homogenized pyroxene are $^{[6]}Ti^{4+}$-$2^{[4]}Al^{3+}$ and $^{[6]}Cr^{3+}$-$^{[4]}Al^{3+}$ in equal proportions. Trace element compositions in unequilibrated eucrites are variable because of igneous zoning, but averaged analyses show core-rim differences that reflect their Ca-rich rims relative to Ca-poor cores. The pyroxene REE abundances in the unequilibrated samples are as much as ten times chondrite in their rims, whereas homogenized Juvinas pyroxenes have abundances between the core and rim values of pyroxene from unequilibrated eucrites.

The ratio of REEs (homogenized pyroxene/bulk composition) for Juvinas is significantly higher than the ratio of REEs (pyroxene cores/bulk composition) for the unequilibrated eucrites. This is especially true for the HREEs. The higher observed REE concentrations in the equilibrated pyroxene result from the intracrystalline exchange between Ca-poor cores and Ca-rich rims and also from intercrystalline exchange with other phases, including plagioclase, phosphates, and mesostasis. Use of the equilibrated pyroxene REE concentrations and igneous D values leads to an incorrect estimate of the parental melt composition. The estimated chondrite-normalized melt REE concentrations are too high by a factor of two to four. These studies suggest that great care must be used to take into account subsolidus elemental redistributions when attempting to estimate parental melt compositions from measured mineral trace element concentrations.

Introduction

Eucrites, diogenites, and howardites are meteorites considered to have formed from magmatic activity and impact brecciation on an asteroidal parent body, probably 4 Vesta, ~4.6 b.y. ago (Consolmagno and Drake 1977; Drake 1979; Binzel and Xu 1993). These related meteorite types are known as the HED association. Eucrites are composed of approximately equal proportions of pyroxene and plagioclase. Diogenites are orthopyroxenites, and howardites are polymict breccias containing eucritic and diogenitic material (e.g., Mason 1967; Stolper 1977; Grove and Bartels 1992).

Eucrites are classified as cumulate, noncumulate, or polymict by their petrographic and compositional characteristics. Cumulate eucrites are coarse-grained and most contain inverted pigeonite. Their bulk compositions do not represent melt compositions, reflecting a preferential accumulation of plagioclase relative to pyroxene (e.g., Consolmagno and Drake 1977). Noncumulate eucrites represent the ordinary eucrites (monomict or unbrecciated) (Reid 1982; Takeda 1991). Polymict eucrites are breccias of more than one eucrite type in which orthopyroxene, like that found in diogenites, is absent or rare (<10 vol%) and can contain cumulate or noncumulate eucritic clasts, and fragments of equilibrated or unequilibrated eucrites (Reid 1982; Score et al. 1982; Delaney et al. 1984). Unequilibrated and equilibrated eucrites were first defined by Takeda et al. (1976) and Reid and Barnard (1979). Takeda et al. (1976, 1978a) noted the first occurrence of supercooled basalts in the Pasamonte eucrite, which was characterized by a wide range in pyroxene chemistry. Takeda et al. (1978a, 1983a) recognized these Pasamonte-type materials in Antarctic polymict eucrites and termed these materials as unequilibrated, whereas the ordinary

0003–004X/96/1112–1438$05.00

eucrites are considered as equilibrated (Reid and Barnard 1979). Takeda and Graham (1991) further classified the eucritic pyroxene in both Antarctic and non-Antarctic eucrites. They identified compositional and textural relationships of eucritic pyroxene that reflect the degree of homogenization in the pyroxene (types 1–6) and therefore provide a measure of its thermal history. For simplicity, in this study we generally defined unequilibrated eucrites to contain pyroxene without visible exsolution lamellae and to have normal igneous compositional zoning, with a wide range of Mg/(Mg + Fe) atomic = Mg′, from core to rim. Equilibrated eucrites contain pyroxene that may have microscopic or macroscopic exsolution lamellae, have a very narrow range of Mg′, and lack significant compositional zoning.

Pyroxene is one of the dominant phases in eucrites and is a sensitive recorder of variables affecting crystallization. Therefore, it is valuable in deciphering the evolution of these meteorites. For example, Bence and Papike (1972), Boyd and Smith (1971), and Grove (1982) showed that major and minor element zoning trends in lunar pyroxene are related to bulk-rock compositions, cooling rates, and intensive thermodynamic parameters (e.g., temperature and f_{O_2}). Using a secondary ion mass spectrometer (SIMS) for the measurement of trace elements, Shearer et al. (1989) reanalyzed some of the mare basalt samples examined by Bence and Papike (1972) to study the trace element behavior in these basalts. In a similar fashion, this study evaluates the major, minor, and trace element systematics of pyroxene from eucritic meteorites to extend our understanding of pyroxene trace element zoning. We also attempt to evaluate the trace element behavior and the effects of reequilibration between the unequilibrated eucrites and the equilibrated eucrites, represented by Juvinas.

Samples and analytical techniques

A total of nine thin sections were selected for analysis, including six thin sections representing five unequilibrated polymict eucrites, all from the Antarctic meteorite collection at the National Institute of Polar Research in Tokyo, Japan [Yamato (Y)-74159,62-1; Y-74450,74-6 and 74-10; Y-75011,96; Y-793548,51-2; and Y-82210,64-1]. Pasamonte (UNM 607), a non-Antarctic sample and also an unequilibrated polymict eucrite, was selected for comparison with the Yamato meteorites. The polymict eucrites selected for study contained eucritic lithic fragments with unequilibrated pyroxene. Juvinas (UNM 210 and UNM 1049), an equilibrated eucrite, was selected for comparison with the unequilibrated eucrites. The Pasamonte and Juvinas samples were provided by the meteorite collection at the Institute of Meteoritics, University of New Mexico.

Pyroxene was examined from all nine thin sections using transmitted and reflected light optical microscopy. Electron microprobe traverses were made across the unequilibrated pyroxene, and selected points were analyzed on equilibrated pyroxene from Juvinas UNM 210 for major and minor element compositions. Analyses were measured with the JEOL 733 Superprobe equipped with a backscattered electron detector, five wavelength spectrometers, and a LINK exL II operating system. Analyses were obtained using mineral and oxide standards at an accelerating voltage of 15 keV, a beam current of 20 nA, and a beam diameter of 1 μm. Wavelength-dispersive peak counting times of 20 s were used for major elements and 40 s for minor elements. Data were reduced with a ZAF correction program.

Pyroxene grains from lithic clasts with clearly evident major element compositional zoning were selected from each of the unequilibrated polymict eucrites, i.e., grains clearly showing Ca-depleted cores and Ca-enriched rims. Also selected for trace element analysis by SIMS were equilibrated pyroxene grains in Juvinas UNM 1049. The unequilibrated pyroxene grains from the polymict eucrites were in eucritic clasts except for Y-74450,74-10, in which only the core of an unequilibrated matrix pyroxene was analyzed. One to three grains from each eucritic fragment were analyzed for trace elements, at core and rim positions along the major element–zoning traverses (measured by the electron microprobe). Major and minor element compositions were measured in both UNM 210 and UNM 1049, whereas trace elements were analyzed in only three grains from UNM 1049. Juvinas has been noted to have three areas with different textures: coarse crystalline, granoblastic, and acicular plagioclase areas (Takeda and Yamaguchi 1991). Pyroxene in Juvinas also shows fine exsolution lamellae and contains numerous inclusions of oxides at the TEM scale (Harlow and Klimentidis 1980; Basaltic Volcanism Study Project 1981; Hanowski and Brearley 1995). The exsolution is often resolvable by electron microprobe but not by SIMS; therefore, trace element analysis integrated both host and lamellae as well as tiny oxide grains.

Trace element analyses were performed using the CAMECA IMS 4f instrument operated by the University of New Mexico and the Sandia National Laboratories Ion Microprobe Facility. The core and rim of each pyroxene grain were analyzed for eight REEs (La, Ce, Nd, Sm, Eu, Dy, Er, Yb) and for Sr, Y, and Zr. The standard used for calibration of the REEs was KH1, Kilbourne Hole Augite (Irving and Frey 1984); the standard used for Sr, Y, and Zr was KAUG, Kakanui Augite (Mason and Allen 1973). Analyses were made by bombardment of the sample with primary O^- ions accelerated through a nominal potential of 10 kV. A primary ion current of 30–40 nA was focused on the sample over a spot diameter of 25–35 μm. Sputtered secondary ions were energy filtered (Shimizu et al. 1978) using a sample offset voltage of −75 V and an energy window of ±25 V to eliminate isobaric interferences, including the interferences of LREE monoxides with Dy, Er, and Yb. Each analysis involved repeated cycles of peak counting on $^{30}Si^+$, $^{88}Sr^+$, $^{89}Y^+$, $^{90}Zr^+$, $^{139}La^+$, $^{140}Ce^+$, $^{146}Nd^+$, $^{147}Sm^+$, $^{151}Eu^+$, $^{153}Eu^+$, $^{163}Dy^+$, $^{167}Er^+$, and $^{174}Yb^+$, as well as counting on a background position to monitor detection noise. Counting times were varied to

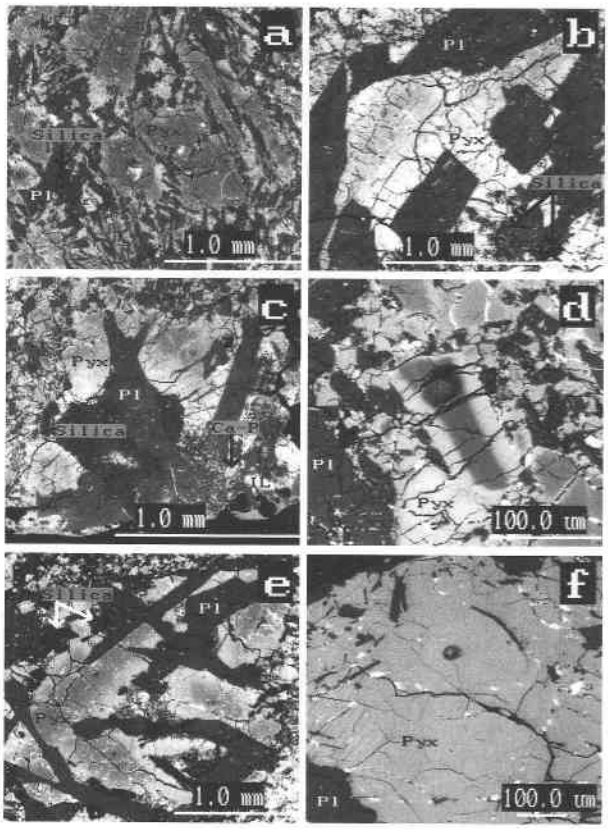

FIGURE 1. BSE images of selected samples showing compositional zoning of pyroxene in the unequilibrated eucrites and equilibrated Juvinas. Pyx = pyroxene, Pl = plagioclase, IL = ilmenite, Ca-P = calcium phosphates. (**a**) Y-82210 showing subophitic texture, (**b**) a coarse-grained clast from Y-74450,74-5, (**c**) an entire lithic clast from Y-793548, (**d**) a matrix pyroxene grain from Y-74450,74-10, (**e**) an entire lithic clast from Pasamonte, and (**f**) an equilibrated pyroxene grain in Juvinas.

achieve an analytical precision of at least 5–10% on each element. The only exception was Eu in some of the Juvinas and Pasamonte pyroxene, which fell below detection limits. Precision from counting statistics was normally better than ±2%. Absolute concentrations of each element were calculated using the empirical relationships between the ratio of measured peak to $^{30}Si^{+}$ (normalized to known SiO_2 content) and elemental concentration as derived from analyses of documented pyroxene standards.

SAMPLE PETROGRAPHY

The analyzed Yamato meteorites are all polymict eucrites, which contain clasts with a variety of basaltic textures. Polymict eucrites are common in Antarctic meteorite collections but rare in non-Antarctic samples. In general, polymict eucrites are fine breccias of lithic fragments, without large clasts. The lithic fragments are mostly eucritic in composition with a variety of basaltic textures, ranging from extremely fine quench textures, ophitic textures, and cumulate textures, to recrystallized and granoblastic textures (Reid 1982).

Three of the selected Yamato eucrites (Y-74159, Y-74450, Y-75011) were previously studied in detail and inferred to be paired (Takeda et al. 1978a, 1978b, 1979, 1983a, 1983b; Miyamoto et al. 1978; Takeda 1987, 1991). Extensive petrographic descriptions of these eucrites, from Delaney et al. (1984) and Takeda and Yanai (1982), are summarized below. Y-74159 and Y-74450 contain small but abundant angular lithic clasts and mineral fragments. Clasts are up to approximately 1 cm in diameter. The lithic clasts are basaltic (equal proportions of pyroxene and plagioclase) and show a range of textures but a limited range of chemical compositions. The clasts have textures representing both rapid cooling (like those of Pasamonte) and slow cooling (implied by pigeonite with exsolution lamellae and blebs). The matrix is comminuted pyroxene and plagioclase mineral fragments. Takeda et al. (1979) noted that Y-75011 contains rare fragments of inverted pigeonite, similar to those in the cumulate eucrites Binda and Moama; similar fragments were found in both Y-74159 and Y-74450. Takeda et al. (1983b) reported that Y-75011, Y-75015, Y-74159, and Y-74450 are paired.

Y-82210 contains abundant coarse-grained basaltic clasts up to 5 mm across and a few areas of brecciated, granular crystals of pyroxene and plagioclase set in a fine-grained, fragmental matrix (Graham and Yanai 1986; Yamaguchi and Takeda 1992). Y-793548 is a fragmental breccia rich in lithic clasts and fine-grained comminuted matrix (Yamaguchi and Takeda 1992). Four types of lithic clast are present: (1) fine-grained variolitic to subophitic basalts with chemically zoned pyroxene and plagioclase; (2) coarse-grained basalts with plagioclase and pyroxene; (3) glass; and (4) porphyries of pyroxene phenocrysts set in very fine-grained variolitic groundmass of pyroxene and plagioclase.

Our thin-section suites of these meteorites match these descriptions in the literature. Details of the individual analyzed clasts follow. Y-82210,61-4 contains basaltic clasts with subophitic textures. A third of this thin section is a basalt clast that cooled quickly, with subophitic texture (Fig. 1a). The section also contains radiating pyroxene and plagioclase (variolitic texture) and domains of plagioclase ophitically enclosed by pyroxene. Pyroxene grains, to 1.6 × 6.4 mm, are clear, subhedral, twinned, and compositionally zoned. Plagioclase grains are twinned, with undulatory extinction, and range from small blocky laths to long thin laths (0.06 × 0.8 mm). The mesostasis is rich in silica, iron nickel metal, troilite, and ilmenite.

Y-74450,74-6 contains several coarse-grained eucrite fragments and clasts with radiating plagioclase and pyroxene grains. The analyzed clast is coarse grained and dominated by plagioclase laths (0.4 × 1.0 mm). Its pyroxene grains are zoned and appear interstitial among the plagioclase grains. There is also a small region of dark mesostasis dominated by silica, disseminated troilite, and

TABLE 1. Average (core and rim) electron microprobe analyses of pyroxene grains

	Y-82210 core	Y-82210 rim	Y-793548 core	Y-793548 rim	Y-74450 core	Y-74450 rim	Y-74159 core	Y-74159 rim	Y-75011 core	Y-75011 rim	Pasamonte core	Pasamonte rim	Juvinas avg.
							Weight percent						
SiO_2	52.1	49.8	51.7	48.7	53.4	49.0	52.1	47.1	50.4	47.6	51.5	48.3	49.4
Al_2O_3	1.74	1.66	1.17	0.973	1.02	1.38	1.97	1.24	1.41	1.17	1.62	1.16	0.420
TiO_2	0.206	0.571	0.171	0.449	0.157	0.664	0.237	0.738	0.248	0.517	0.160	0.421	0.240
Cr_2O_3	0.941	0.566	0.637	0.369	0.811	0.534	0.959	0.309	0.837	0.521	0.768	0.658	0.460
MgO	22.3	12.2	19.6	9.55	25.6	9.78	23.0	5.71	17.0	8.35	19.9	9.18	12.3
FeO	18.8	25.8	22.1	30.6	16.3	25.3	17.7	33.7	23.7	30.3	21.2	30.1	30.6
MnO	0.654	0.850	0.707	0.992	0.458	0.813	0.627	1.23	0.818	1.06	0.733	0.973	0.890
CaO	2.83	8.82	3.36	7.74	1.68	12.1	2.82	9.00	4.51	9.01	3.12	8.17	5.26
Na_2O	0.002	0.026	0.002	0.013	0.000	0.057	0.002	0.021	0.000	0.006	0.000	0.007	0.000
Total	99.53	100.20	99.45	99.40	99.46	99.63	99.44	99.01	98.96	98.51	99.08	98.94	99.51
Si (afu)	1.940	1.941	1.960	1.958	1.957	1.941	1.931	1.946	1.946	1.944	1.950	1.952	1.966
$^{[4]}Al$	0.060	0.059	0.040	0.041	0.042	0.059	0.069	0.051	0.052	0.055	0.050	0.048	0.020
Total tetrahedral	2.000	2.000	2.000	1.999	1.999	2.000	2.000	1.997	1.998	1.998	2.000	1.999	1.986
$^{[6]}Al$	0.016	0.017	0.012	0.005	0.002	0.005	0.017	0.009	0.013	0.002	0.023	0.008	0.000
Ti	0.006	0.017	0.005	0.014	0.004	0.020	0.007	0.023	0.007	0.016	0.005	0.013	0.007
Cr	0.028	0.017	0.019	0.012	0.023	0.017	0.028	0.010	0.026	0.017	0.023	0.021	0.014
Mg	1.235	0.704	1.104	0.573	1.397	0.577	1.271	0.351	0.975	0.508	1.124	0.551	0.727
Fe	0.584	0.840	0.700	1.031	0.499	0.839	0.550	1.164	0.770	1.033	0.673	1.017	1.020
Mn	0.021	0.028	0.023	0.034	0.014	0.027	0.020	0.043	0.027	0.037	0.024	0.033	0.030
Ca	0.113	0.370	0.137	0.334	0.066	0.512	0.112	0.398	0.187	0.394	0.127	0.355	0.224
Na	0.000	0.002	0.000	0.001	0.000	0.004	0.000	0.002	0.000	0.001	0.000	0.001	0.000
M1 + M2	2.002	1.996	2.000	2.001	2.006	2.001	2.005	2.000	2.003	2.006	1.997	1.998	2.024
Fe/(Mg + Fe)	0.32	0.55	0.39	0.64	0.26	0.59	0.30	0.77	0.44	0.67	0.37	0.65	0.58
Wo (mol%)	5.84	19.38	7.05	17.2	3.36	26.5	5.79	20.8	9.67	20.4	6.59	18.4	11.4
En	63.9	36.7	56.9	29.6	71.2	29.9	65.7	18.3	50.5	26.2	58.4	28.7	36.9
Fs	30.2	43.9	36.1	53.2	25.4	43.5	28.5	60.9	39.8	53.4	35.0	52.9	51.7
No. of EMP analyses	8	5	7	4	2	2	4	4	9	7	10	12	34

Note: Pyroxene grains are from the Yamato meteorites, Pasamonte UNM 607, and Juvinas (Basaltic Volcanism Study Project 1981).

iron nickel metal (Fig. 1b). Only a matrix pyroxene with an Mg-rich core was analyzed in Y-74450,74-10 (Fig. 1d).

Y-793548,51-2 is weathered and its clasts are stained by iron oxides. The section exposes numerous fine- and coarse-grained basalt clasts set in a brecciated matrix of pyroxene and plagioclase mineral fragments. The examined clast within Y-793548 is coarse grained with clear, compositionally zoned pyroxene (up to 0.5 × 0.6 mm), twinned elongated plagioclase laths (0.2 × 1.3 mm), and mesostasis containing silica, ilmenite, and rare calcium phosphates (Fig. 1c).

Section Y-75011,96 is from a large coarse-grained eucrite clast with ophitic texture, possibly the same as studied by Takeda et al. (1983a, 1983b, 1994) and Takeda and Graham (1991) in Y-75011,84. The pyroxene grains in Y-75011,84 are identified to be of the most unequilibrated type (type 1), whereas those found in Y-75011,96 are more equilibrated (H. Takeda 1996, personal communication) according to the pyroxene-homogenization classification of Takeda and Graham (1991). The clast is mostly of ophitic texture, with domains of variolitic texture (radiating pyroxene and plagioclase laths). Pyroxene grains (1.8 × 0.4 mm) are slightly clouded and compositionally zoned; plagioclase grains are lath shaped (0.4 × 2.2 mm). The dark mesostasis consists of silica, ilmenite, troilite, and rare iron nickel metal.

Y-74159,62-1 is dominated by a large eucrite clast with variolitic texture. Pyroxene grains (1.2 × 2.9 mm) are subhedral and clear, with compositional zoning. Plagioclase grains are twinned and range from blocky to long lath shapes (up to 0.5 × 1.4 mm). The dark mesostasis is dominated by disseminated silica, ilmenite, troilite, and iron nickel metal.

Pasamonte UNM 607 and Juvinas UNM 1049 were selected for comparison with the Antarctic polymict eucrites. Pasamonte was recently redescribed as a polymict eucrite (Metzler et al. 1994, 1995). Pasamonte UNM 607 contains eucritic clasts with textures ranging from fine to moderately coarse grained. This study concentrated on pyroxene from an unequilibrated, moderately coarse-grained eucrite clast with subophitic texture that has minor silica-rich mesostasis (Fig. 1e). Pyroxene grains are clear, subhedral, twinned, and compositionally zoned (1.5 × 0.6 mm). Plagioclase grains are clouded, twinned, and lath shaped (0.4 × 1.3 mm). Juvinas UNM 1049 is a brecciated equilibrated eucrite containing subophitic to ophitic lithic fragments. Regions of the thin section are composed of pyroxene grains embedded in fine-grained subophitic melt regions characterized by fine acicular plagioclase grains (Takeda and Yamaguchi 1991; Metzler et al. 1995). Pigeonite (0.4 × 0.9 mm) of uniform composition, and commonly twinned and clouded with chromite, contains prominent, fine exsolution lamellae of augite on the (001) planes of the host (Takeda and Graham 1991; Fig. 1f). Plagioclase laths are clouded and up to 0.3 × 1.0 mm.

PYROXENE MAJOR AND MINOR ELEMENT SYSTEMATICS

Compositional zoning in pyroxene is observed petrographically (Fig. 1) and confirmed by electron micropro-

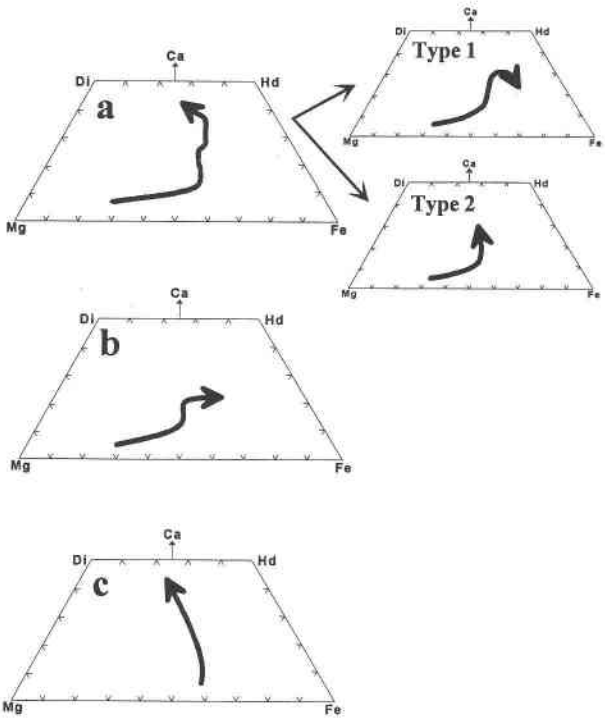

FIGURE 2. Schematic quadrilaterals illustrating the primary chemical zoning trends of pyroxene found in many Antarctic eucrite samples. Lines represent generalized distribution of data obtained from core-to-rim microprobe traverses (Takeda et al. 1983a; Miyamoto et al. 1985; Takeda and Graham 1991). The Mg-Fe-Ca trend (**a**) is typical of Pasamonte where zoning of pigeonite is from Mg-rich cores to Fe-rich rims. Type 1 zoning is common in pyroxene adjacent to mesostasis, whereas type 2 zoning typically occurs in pyroxene adjacent to surrounding plagioclase crystals. The Mg-Fe trend (**b**) is typical of chemical zoning in Y-75011. The Fe-Ca trend (**c**) is the chemical variation simulating the tie-line trends from host pigeonite to exsolved augite of ordinary eucrites.

be data. Average electron microprobe analyses of pyroxene cores and rims from near the SIMS pits in the unequilibrated polymict eucrites and pyroxene from Juvinas (Basaltic Volcanism Study Project 1981) are listed in Table 1. Takeda et al. (1983b) identified three distinct chemical zoning trends in the pyroxene of eucrites, and these trends are described in more detail in Takeda and Graham (1991). In general, these trends are found in more quickly cooled basalts containing pyroxene that has not exsolved on a microprobe scale. These magmatic or subsolidus trends (Fig. 2) are (Fig. 2a) the Pasamonte trend (Mg-Fe-Ca trend), (Fig. 2b) the Y-75011 trend (Mg-Fe trend), and (Fig. 2c) the Y-790266 trend (Fe-Ca trend). Takeda et al. (1982, 1983b) also noted that the chemical zoning in pyroxene depends primarily on the bulk chemistry of the basaltic melt and on crystal-growth conditions such as the degree of supercooling and nucleation density. Erasure of chemical zoning may result from either slow cooling in a continuous cooling process or equilibration by a late, secondary high-temperature event (e.g., impact).

The Pasamonte trend reflects zoning from Mg-rich pigeonite cores to more Ca- and Fe-rich augite rims (Fig. 2a) and has two subtypes. Type 1 typically occurs in pyroxene adjacent to mesostasis regions, whereas type 2 zoning typically occurs in pyroxene adjacent to surrounding plagioclase crystals (Fig. 2a). The Pasamonte trend was found in Y-74159, Y-74450,74-6, Y-82210, Y-793548, and Pasamonte (Fig. 3). Note that Y-74450,74-6 ("A1") has more Ca-rich pigeonite and therefore may only represent the Fe-Ca extension of the Mg-Fe-Ca trend, whereas "D" in Y-74450,74-10 is an analysis of a matrix pyroxene that is represented by an Mg-rich core (Fig. 3).

The chemical variation from core to rim for pyroxene adjacent to dark mesostasis is gradual in the Y-75011 trend (Fig. 2b). This Mg-Fe trend has more Fe enrichment and less Ca enrichment (Fig. 2b) than the Pasamonte trend and was observed in the clasts of Y-75011,96 (Fig. 3). Note that the zoning trend of Y-75011,96 (Fig. 3) is less Mg rich than that observed for Y-75011,84 (Takeda et al. 1983a, 1994) because Y-75011,96 is more equilibrated.

The Y-790266 trend results from electron microprobe beam overlap of host pigeonite and exsolved augite in ordinary equilibrated eucrites (Fig. 2c). The pyroxene homogenization occurred prior to exsolution (Basaltic Volcanism Study Project 1981). Juvinas UNM 210 exemplifies this trend of homogenization but now is composed of two pyroxenes and iron oxides in fine intergrowth (Fig. 3).

Electron microprobe traverses across pyroxene grains of the polymict eucrite lithic fragments also illustrate the major and minor element zoning (Fig. 4). These pyroxene grains show normal igneous zoning, where Mg is enriched in the cores and Fe and Ca are enriched in the rims as crystallization proceeds. Minor element patterns are more erratic, but in general Cr and Al decrease in the rims, whereas Ti increases in the rims.

In eucritic pyroxene, Cr, Al, and Ti are the important minor element cations (Papike and Cameron 1976). Assuming that most Ti is Ti^{4+}, not Ti^{3+}, and enters the M1 site instead of the tetrahedral site, that Cr is trivalent not divalent, and that Na can be ignored because of its low concentration, a charge-balance equation can be written as follows: octahedral site charge excess relative to quadrilateral = tetrahedral site charge deficiency relative to quadrilateral, or $^{[6]}Al^{3+} + {}^{[6]}Cr^{3+} + 2{}^{[6]}Ti^{4+} = {}^{[4]}Al^{3+}$.

The primary substitutional couples among Cr, Al, and Ti are as follows: (1) $^{[6]}Cr^{3+}$-$^{[4]}Al^{3+}$, (2) $^{[6]}Al^{3+}$-$^{[4]}Al^{3+}$, and (3) $^{[6]}Ti^{4+}$-$2^{[4]}Al^{3+}$. Using the pyroxene from the analyzed grains of Y-82210 and Juvinas UNM 210 as examples of Cr-Al-Ti systematics, Figure 5 plots the covariation of Ti and the Al that is not associated with the $^{[6]}Cr^{3+}$-$^{[4]}Al^{3+}$ couple. If all the Ti were tetravalent and all the Ti and Al were incorporated into the couple $^{[6]}Ti^{4+}$-$2^{[4]}Al^{3+}$, these grains would plot on the trend with Ti/Al = ½. If the couples were solely $^{[6]}Al^{3+}$-$^{[4]}Al^{3+}$, the grains would plot

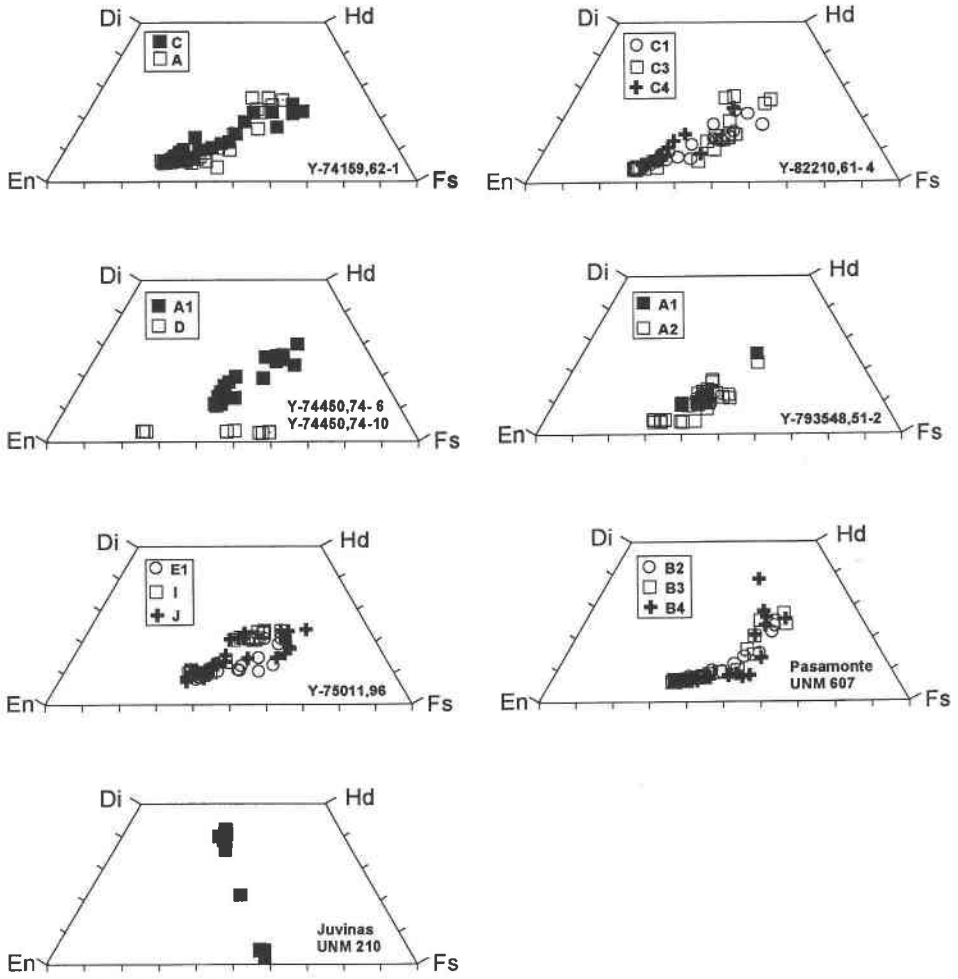

FIGURE 3. Pyroxene quadrilateral compositions from unequilibrated grains and Juvinas UNM 210.

along the x axis. If the $^{[6]}Ti^{4+}$-$2^{[4]}Al^{3+}$ and $^{[6]}Al^{3+}$-$^{[4]}Al^{3+}$ couples were equally abundant, then the plotted points from these grains would fall on a slope of Ti/Al = ¼. In Figure 5a, the points from grain C4 mostly plot below the ¼ slope line, with increasing substitutions from core to rim, indicating that one of the important couples of minor elements in this pyroxene, after the $^{[6]}Cr^{3+}$-$^{[4]}Al^{3+}$ couple, is the $^{[6]}Al^{3+}$-$^{[4]}Al^{3+}$ couple. The pyroxene from grains C1 and C3 shows that the dominant initial couple is $^{[6]}Al^{3+}$-$^{[4]}Al^{3+}$, which correlates with magnesian core compositions. As plagioclase starts to crystallize, there is an upturn of the crystallization path, and $^{[6]}Ti^{4+}$-$2^{[4]}Al^{3+}$ becomes dominant over $^{[6]}Al^{3+}$-$^{[4]}Al^{3+}$ in the rims of the pyroxene, because the Al in the melt is incorporated into the plagioclase in competition with the pyroxene. Figure 5b reflects the homogenized and equilibrated nature of Juvinas. All the Al that is not coupled with Cr falls along the Ti/Al = ½ slope, indicating that reequilibration erased the $^{[6]}Al^{3+}$-$^{[4]}Al^{3+}$ couple. The loss of the $^{[6]}Al^{3+}$-$^{[4]}Al^{3+}$ couple during pyroxene crystallization is taken up by the crystallization of plagioclase.

Crystallization sequences can be summarized in ternary plots of the three types of substitutional couples for each of the grains analyzed with an average from Juvinas UNM 210 for comparison (Fig. 6). With the exceptions of Y-82210 C4 and Y-74450 D, all the pyroxene grains from the unequilibrated polymict eucrite samples show that as plagioclase starts to crystallize after pyroxene is already crystallizing, the dominant couple proceeds from $^{[6]}Cr^{3+}$-$^{[4]}Al^{3+}$ in the cores of the pyroxene grains toward $^{[6]}Ti^{4+}$-$2^{[4]}Al^{3+}$ in the rims. Y-82210 C4 shows that as the pyroxene crystallizes, the dominant substitutional couple is $^{[6]}Cr^{3+}$-$^{[4]}Al^{3+}$, followed by $^{[6]}Al^{3+}$-$^{[4]}Al^{3+}$, where the crystallization path is continuous without the onset of plagioclase crystallization. The analysis of Y-74450 D primarily represents the core of the grain and therefore dominantly reflects the initial $^{[6]}Cr^{3+}$-$^{[4]}Al^{3+}$ couple. The dominant substitutional couples for Juvinas UNM 210, representing equilibrated pyroxene, are $^{[6]}Ti^{4+}$-$2^{[4]}Al^{3+}$ and $^{[6]}Cr^{3+}$-$^{[4]}Al^{3+}$ in equal proportions, as demonstrated in Figures 5b and 6. However, these components now represent two pyroxenes and oxide phases in Juvinas. The Al, Ti, and Cr

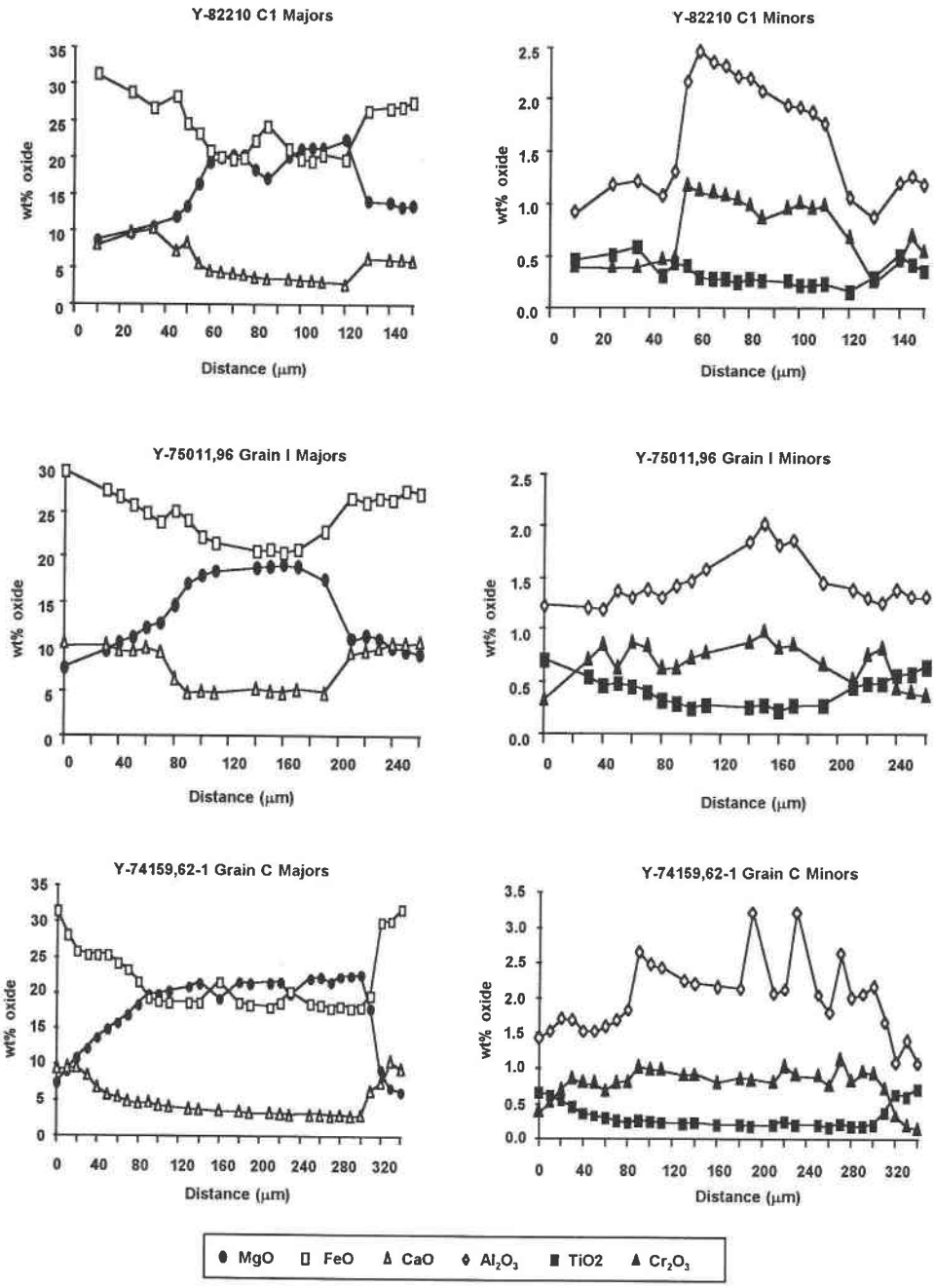

FIGURE 4. Major and minor element electron microprobe traverses from representative pyroxene grains in unequilibrated eucrite clasts showing compositional zoning from rim to rim.

chemical zoning trends appear to have homogenized upon reequilibration, as indicated by the small region of the ternary diagram in which the Juvinas data plot as contrasted with the wide range of compositions for the unequilibrated samples. The change in Ti/Al trends from <¼ to ½ in unequilibrated pyroxene can be used as an indicator of plagioclase saturation and crystallization. This conclusion is consistent with the findings of Bence and Papike (1972) for lunar pyroxene.

On the basis of the pyroxene quadrilaterals, the Ti/Al systematics, and the ternary plots of Al, Cr, and Ti, we interpret the crystallization trends to be (1) crystallization of pigeonite followed by pigeonite and augite, and (2) simultaneous crystallization of pyroxene and plagioclase. Pyroxene from samples Y-82210 C4 and Y-74450 D reflects the initial onset of pyroxene crystallization and may have stopped crystallizing prior to the onset of plagioclase (Fig. 6).

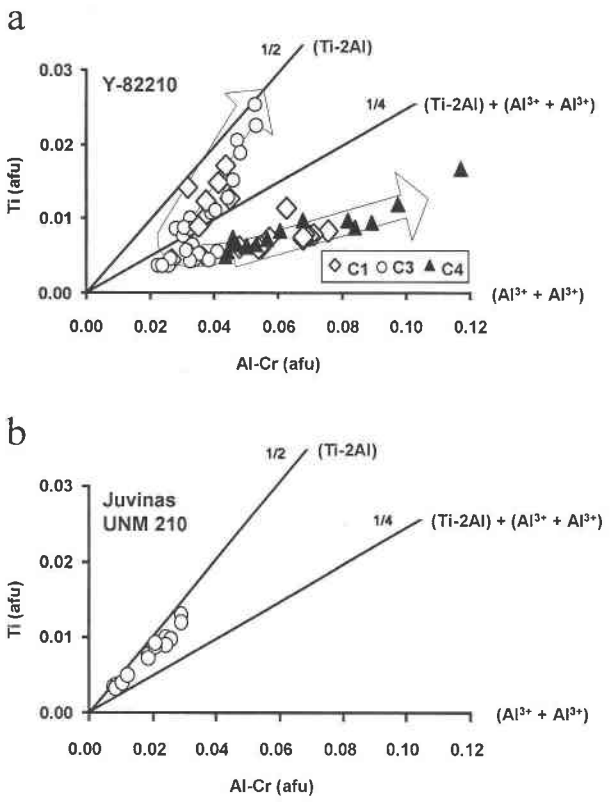

FIGURE 5. Covariation of Al-Cr and Ti, in atoms per formula unit (afu), in the pyroxene grains from Y-82210 and Juvinas UNM 210. Al-Cr represents the Al that is not incorporated into the charge-balance couple $^{[6]}Cr^{3+}$-$^{[4]}Al^{3+}$. (**a**) Arrows indicate crystallization trends as pyroxene grows from core to rim in Y-82210. (**b**) Analyses of pyroxene from Juvinas represent host pigeonite, augite lamellae, and integrated host and lamellae.

PYROXENE TRACE ELEMENT SYSTEMATICS

Pyroxene (core and rim) trace element concentrations for all the analyzed samples show significant variations (Table 2). Individual core analyses show less variation than rim analyses, and the LREE, Sr, Y, and Zr concentrations are more variable than those of the HREEs. Several Antarctic samples also showed positive Ce anomalies. These Ce anomalies were found to be variable in eucrites, with both positive and negative anomalies, and in various regions of the mineral grains analyzed. They are considered to be the result of terrestrial weathering (Shimizu et al. 1983; Floss and Crozaz 1991). Ce anomalies measured in our samples were removed, and only interpolated Ce values were used in calculations. Y-74450,74-10 D contains the most Mg-rich core measured among all the Yamato samples, and the trace element abundances are correspondingly the lowest measured. The average trace element abundances from Juvinas UNM 1049 are also given for comparison with the equilibrated eucrites. Note that the average trace element concentrations for equilibrated Juvinas UNM 1049 are generally between the concentrations of cores and rims in the unequilibrated polymict eucrites. Some variability in rim and core concentrations in the unequilibrated pyroxene may result from integration of compositional zoning within the SIMS analysis volumes.

CI-normalized (Anders and Grevesse 1989) trace element patterns for average core and rim analyses of unequilibrated pyroxene grains from the different polymict eucrites are generally similar, with some subtle variations (Fig. 7). All the Yamato pyroxene analyses have trace element abundances up to approximately ten times CI, with Y-75011 rims having the highest abundances (up to 12.1 times CI for Yb). The most Mg-rich core sample (Y-74450,74-10 D) has the lowest REE abundances, with La to only 0.04 times CI. Among the Yamato samples, the core REE abundances range to only 3.2 times CI.

TABLE 2. SIMS analyses of pyroxene grains

	Y-82210 core	Y-82210 rim	Y-793548 core	Y-793548 rim	Y-74450 core	Y-74450 rim	Y-74159 core	Y-74159 rim	Y-75011 core	Y-75011 rim	Pasamonte core	Pasamonte rim	Juvinas* avg.
						Parts per million							
Sr	0.392	4.23	0.575	3.882	0.123	4.16	0.406	3.04	0.444	5.61	0.200	2.02	0.119
Y	3.77	12.9	3.34	14.48	1.92	15.6	3.42	17.2	4.80	19.4	2.03	8.47	7.49
Zr	2.18	20.8	2.60	15.36	1.44	11.3	3.72	14.3	2.74	20.8	1.23	5.23	7.89
La	0.044	0.704	0.063	0.237	0.010	0.177	0.017	0.265	0.058	0.74	0.004	0.090	0.030
Ce	0.196	2.07	**	1.14	**	1.21	0.073	0.94	**	2.74	0.030	0.440	0.146
Nd	0.265	1.88	0.230	1.447	0.089	1.56	0.110	1.75	0.324	2.65	0.061	0.633	0.305
Sm	0.171	0.776	0.129	0.774	0.049	0.897	0.079	0.997	0.193	1.245	0.088	0.432	0.198
Eu	0.014	0.111	0.014	0.086	0.008	0.069	0.006	0.373	0.015	0.150	*<0.008*	0.038	0.026
Dy	0.483	1.65	0.387	1.946	0.196	2.10	0.397	2.17	0.544	2.46	0.241	1.08	0.802
Er	0.324	1.04	0.349	1.217	0.165	1.24	0.323	1.48	0.430	1.70	0.228	0.681	0.718
Yb	0.421	1.12	0.386	1.390	0.190	1.48	0.344	1.52	0.516	1.97	0.269	0.953	0.987
No. of SIMS analyses	3	3	2	2	1	1	2	2	3	3	3	3	3

Note: Pyroxene grains are from the Yamato meteorites, Pasamonte UNM 607, and Juvinas UNM 1049. Italicized trace element concentration indicates detection limit, as noted by the less than symbol.

* Trace elements from Juvinas UNM 1049 (this study).

** Positive Ce anomaly (Shimizu et al. 1983; Floss and Crozaz 1991).

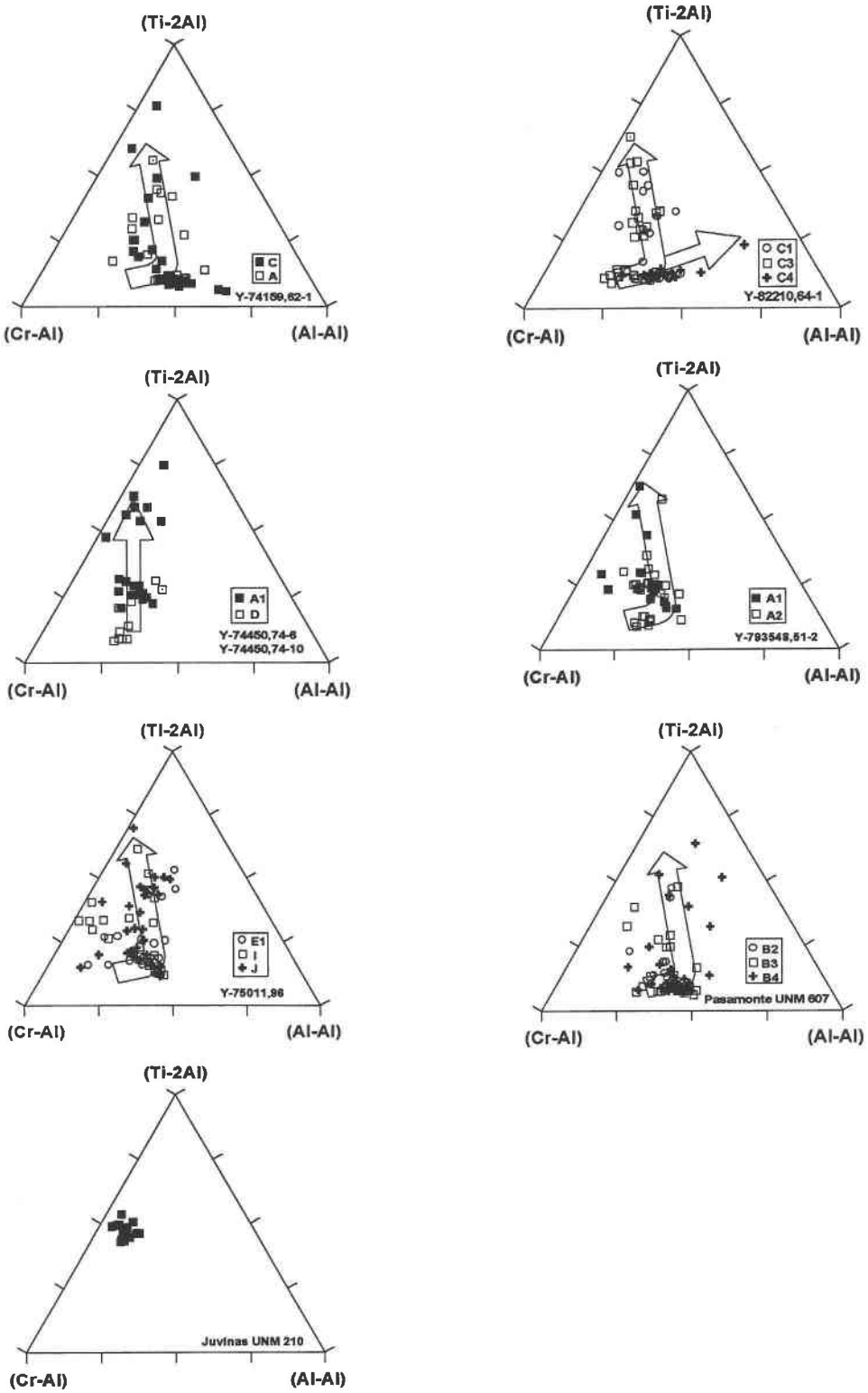

FIGURE 6. Ternary plots of the three types of substitutional couples ($^{[6]}Cr^{3+}$-$^{[4]}Al^{3+}$, $^{[6]}Al^{3+}$-$^{[4]}Al^{3+}$, and $^{[6]}Ti^{4+}$-$2^{[4]}Al^{3+}$) for each of the grains analyzed. The average grain compositions from Juvinas UNM 210 are shown for comparison with grains that are composed of fine intergrowths of two pyroxenes and oxides. Arrows indicate direction of crystallization from core to rim. All the arrows are similar except for Y-82210 C4, indicating pyroxene crystallization without the onset of plagioclase crystallization, and Y-74450 D primarily represents the core of the grain and therefore dominantly reflects the initial $^{[6]}Cr^{3+}$-$^{[4]}Al^{3+}$ couple.

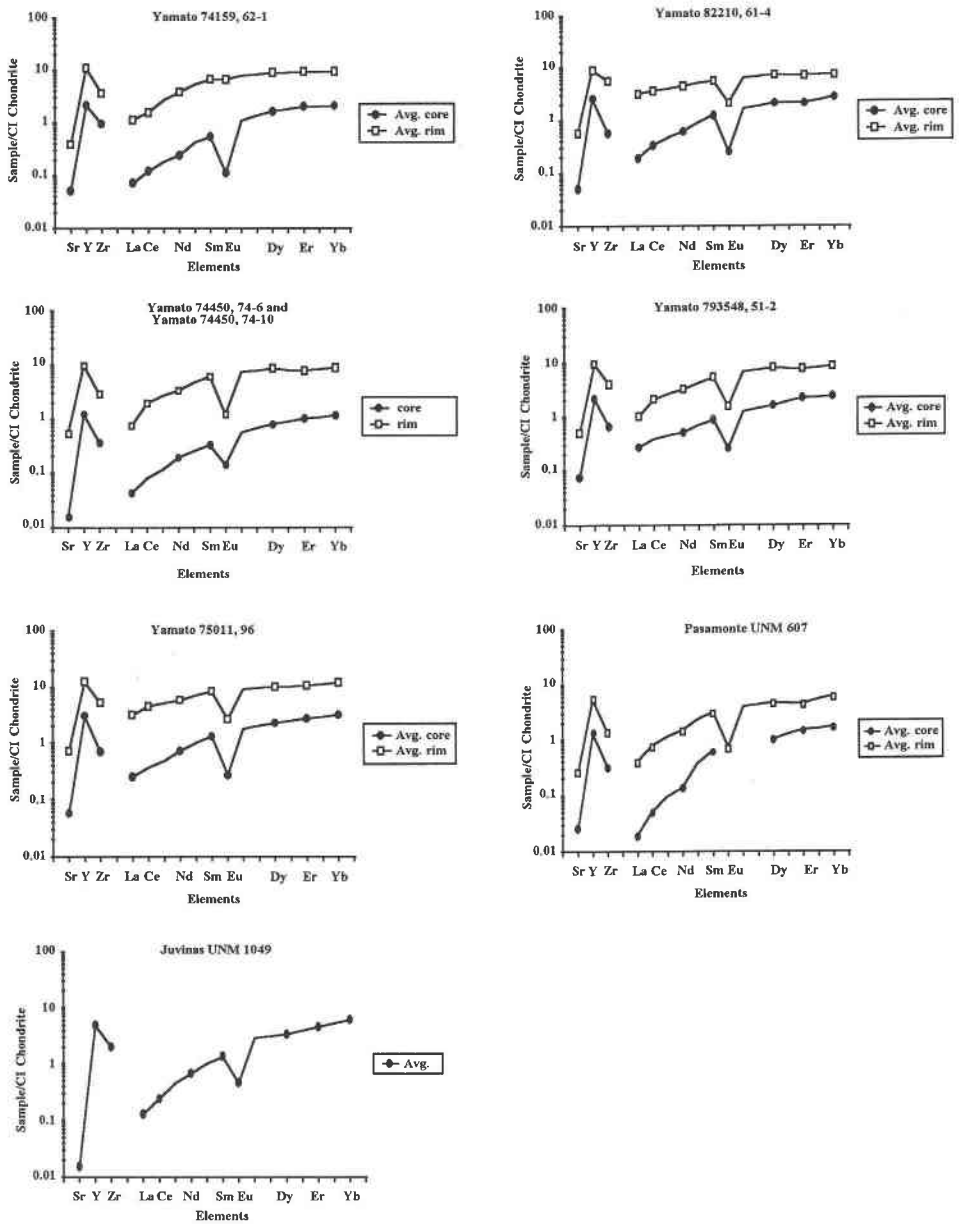

FIGURE 7. CI-normalized (Anders and Grevesse 1989) average trace element analyses of the analyzed grains. Gadolinium was estimated, and some anomalous Ce data points were removed (see text).

The REE patterns of the pyroxene are typical of both Ca-poor and Ca-rich pyroxene. The HREEs are preferentially incorporated into the pyroxene crystal structures relative to the LREEs, giving the LREEs steeper slopes than the HREEs (Shearer et al. 1989). Also, REE abundances are higher for Ca-rich pyroxene than for Ca-poor pyroxene in the unequilibrated grains. The cores of the unequilibrated pyroxene grains have lower REE abundances than the rims. Also note that Sr follows Ca, reflecting their geochemical similarities, and Y and Zr behave like the HREEs in all the samples.

DISCUSSION

Major, minor, and trace element systematics of pyroxene from unequilibrated eucrites

REE systematics of pyroxenes reflect their crystal structures, as described by Shearer et al. (1989) and Pun and Papike (1995). Basically, the REEs enter only the M2 site in pyroxene because the M1 site cannot expand to accommodate these large cations. The M2 site in orthopyroxene cannot expand much; however, the M2 site in augite and pigeonite is more flexible and can accommo-

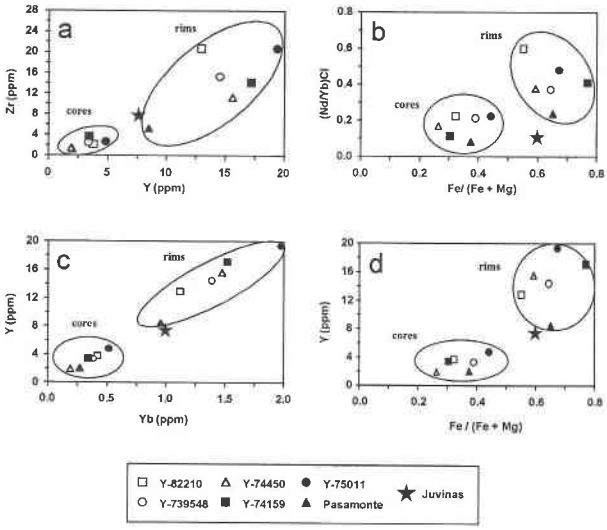

FIGURE 8. (**a**) Zr vs. Y from averaged analyses. A positive correlation was observed between the two elements. (**b**) $(Nd/Yb)_{CI}$ (normalized) vs. Fe/(Fe + Mg) from averaged analyses. Note that all the core-rim pairs increase in $(Nd/Yb)_{CI}$ with increasing Fe/(Fe + Mg). (**c**) Y vs. Yb from averaged analyses. The positive correlation is a result of the geochemical similarities of the two elements. (**d**) Y vs. Fe/(Fe + Mg) from averaged analyses.

date either larger ions such as Ca^{2+} and Na^{+} in eightfold coordination or smaller ions such as Mg^{2+} in sixfold coordination (Takeda 1972; Cameron and Papike 1981). Shearer et al. (1989) and Pun and Papike (1995) showed that Ca-rich pyroxene can hold more REEs than Ca-poor pyroxene because of its larger M2 site. Ca in the augite structure has been experimentally shown to "prop" open the M2 site and, thus, increase the REE abundances (McKay 1989).

Eu abundances in pyroxene are strongly influenced by f_{O_2} during crystallization (McKay 1989; Crozaz and McKay 1989). Eu^{2+} is large and is typically excluded from the M2 site, whereas Eu^{3+} is more readily accommodated. The eucrites studied here formed in a reducing environment similar to the environment in which lunar rocks crystallized (e.g., Stolper 1977); therefore, Eu is found primarily in the Eu^{2+} state, producing the observed negative Eu anomaly.

The other trace elements, Sr, Y, and Zr, behave similarly among all the samples analyzed. These elements are less abundant in Ca-poor pyroxene than in Ca-rich pyroxene, reflecting crystal-chemical constraints on their behavior analogous to those on the REEs. Sr systematically follows Ca, again reflecting the geochemical similarity of the two elements. Y is similar to the HREEs and is more compatible than the LREEs. Zr generally follows Y, and these elements are found in similar abundances (Fig. 8a). Juvinas contains intermediate Zr and Y abundances that plot along a positive trend between the cores and rims of the unequilibrated eucrites.

As crystallization proceeds from core to rim, the pyroxene grains were observed to become enriched in Fe, Ca, and REEs (Fig. 7, Tables 1 and 2). The ratio of LREE/HREE also increases from core to rim as crystallization proceeds for two reasons: (1) The Ca-rich pyroxene rims can accommodate more LREEs (Fig. 8b), and (2) more of the HREEs go into the early pigeonite, thus enriching the residual melt in LREEs. If Nd is used as a representative LREE and Yb as a representative HREE, the $(Nd/Yb)_{CI}$ ratio is positively correlated with Fe/(Fe + Mg) in the unequilibrated pyroxene. Some of the variability in $(Nd/Yb)_{CI}$ may result from SIMS analytical areas that are not the most magnesian identified by EMP and also from the large spot volume extending over highly zoned rims. Juvinas has Fe/(Fe + Mg) intermediate between the cores and rims of the unequilibrated pyroxene but a relatively low $(Nd/Yb)_{CI}$ ratio in comparison with the other samples.

Y and Yb are strongly correlated (Fig. 8c) as expected from their geochemical similarity. All the pyroxene cores have low Y and Yb, whereas rims are enriched in both. Average Juvinas falls in the trend of positive correlation with intermediate concentrations, suggesting that concentrations of both elements were homogenized during equilibration of the pyroxene grains. Y is also correlated with Fe/(Fe + Mg) and may be used as an index of fractionation (Fig. 8d). The crystallization sequence would be as follows: Y-74450, Y-74159, Y-82210, Pasamonte, Y-793548, and Y-75011. This sequence would reflect a true fractionation trend only if we had analyzed the most magnesian cores in all samples and if all samples were from the same magma system. This seems highly unlikely.

The effects of equilibration on major, minor, and trace element systematics

Postcrystallization redistribution of elements can seriously affect our ability to use trace elements in mineral phases to estimate parental melt compositions (Schnetzler and Philpotts 1969; Phinney et al. 1993; Pun and Papike 1995; Treiman 1995; Papike 1996). Trace element abundances in minerals that have undergone postcrystallization elemental exchange may provide erroneous parental melt compositions (Treiman 1996). Pun and Papike (1995) demonstrated that the distribution of trace elements between host and lamellae in equilibrated pigeonite in the cumulate eucrites is controlled by the crystal chemistries of orthopyroxene, pigeonite, and augite. They also suggested that postcrystallization processes (e.g., reequilibration, metamorphism, and impact brecciation) can greatly affect the trace element distribution within the associated mineral phases, and that parental melts must be estimated with caution. Treiman (1995) attempted to estimate the effects of subsolidus chemical equilibration with minerals in basalts that had equilibrated below their solidus. He found that the REE abundances are significantly higher than they would be in the presence of magma, and that these abundances can be used erroneously

TABLE 3. Partition coefficients (D) estimated from pyroxene-bulk composition ratio

	1	2	3	4	5
	Y-75011	Pasamonte	Y-74450	Avg. columns 1–3	Juvinas
La	0.011	0.001	0.003	0.005	0.011
Ce	*	0.004	*	0.004	0.020
Nd	0.031	0.010	0.011	0.017	0.057
Sm	0.058	0.042	0.019	0.040	0.114
Eu	0.023	*0.012*	0.012	0.016	0.043
Dy	0.107	0.070	0.050	0.076	0.286
Er	0.139	0.104	0.069	0.104	0.406
Yb	0.178	0.129	0.083	0.130	0.590
Sr	0.006	0.003	0.002	0.004	0.002

Note: Columns 1–3 represent the partition coefficients (D) estimated from average measured abundance of REEs in pyroxene cores determined by SIMS divided by bulk matrix or clast material (Shimizu and Masuda 1986). Column 5 represents the REE abundance in the homogenized pyroxene divided by the bulk-rock composition. Italics represent calculations from detection limits and therefore represent maximum possible values.

* Positive Ce anomaly (Shimizu et al. 1983; Floss and Crozaz 1991).

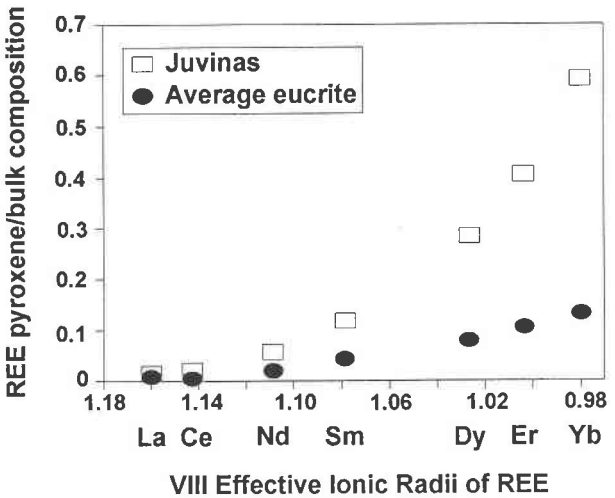

FIGURE 9. The estimated ratio of the REEs (homogenized pyroxene/bulk composition) from Juvinas and from the average eucrite (pyroxene core/bulk composition) represented by Y-75011, Y-74450, and Pasamonte vs. the effective eightfold-coordinated ionic radii of the REEs (Shannon and Prewitt 1970).

to determine the parental melt composition. If a rock equilibrated significantly below its solidus, each mineral phase would provide a different parental magma estimate because of the various temperature dependencies on partition coefficients. Having measured the trace element concentrations in both the unequilibrated eucrites and equilibrated Juvinas, we can now attempt to determine the effects of reequilibration on the behavior of these elements.

In evaluating the petrogenetic relationships among these unequilibrated eucrites and the other eucrites, the REE abundances in the parental magmas in equilibrium with the most Mg-rich cores of the pyroxene are determined by dividing the pyroxene core compositions by the appropriate partition coefficients to determine melt REE characteristics. To calculate parental melt compositions we need to assume that (1) the pyroxene retains its magmatic REE signature, (2) the pyroxene cores were in equilibrium with the earliest melts, and (3) the appropriate partition coefficients (Ds) are used.

The effects of reequilibration between the unequilibrated and equilibrated pyroxenes can be determined using their trace element inventories. Partition coefficients were estimated by dividing the REE abundances in unequilibrated and equilibrated pyroxenes by the REE abundances determined for the bulk samples (Shimizu and Masuda 1986), assuming that these bulk compositions represent melt compositions. There are many potential pitfalls with these estimates, which are based on small, nonrepresentative samples; however, the estimates are still useful. Partition coefficients for HREEs appear to be most affected (Table 3, Fig. 9). Partition coefficients estimated for Y-75011 and Pasamonte appear somewhat similar, whereas those for Y-74450 are much lower (Table 3). In comparison with the average D calculated for these three unequilibrated eucrites, the estimated partition coefficients for equilibrated Juvinas are much higher, especially for the HREEs. The slope of the curve of the D_{HREE} vs. ionic radii for Juvinas (Fig. 9) is much steeper than that for unequilibrated eucrites. This is probably due to the enrichment in HREEs resulting from equilibration with plagioclase, mesostasis, and phosphate minerals. It may also be due to pyroxene homogenization where the average Juvinas pyroxene has higher Ca contents than the Mg-rich cores used to estimate Ds for the unequilibrated eucrites.

Partition coefficients are often assumed to remain constant during crystallization, but this may not be an appropriate assumption (Colson et al. 1988). Fowler et al. (1995) addressed changes in partition coefficients during crystallization and argued that partition coefficients are a function of temperature, bulk composition, and oxygen fugacity (Colson et al. 1988; McKay 1989). Many of these parameters are not well constrained, and there is still a lack of understanding of how partition coefficients change during crystallization. These assumptions clearly ignore the effects of postcrystallization elemental exchange. If the effects of equilibration on the REEs are significant, as they appear to be for the HREEs in Juvinas, then interpretations of parental melt compositions may be seriously compromised. Figure 10 illustrates the effects of reequilibration on estimated parental melt for Juvinas. The hypothetical melt REEs calculated using Ds determined from the unequilibrated eucrites in this study (Table 3, column 4) and REE concentrations of equilibrated Juvinas pyroxene are two to four times more enriched than those of bulk Juvinas. This estimate is incorrect and higher than bulk Juvinas (Shimizu and Masuda 1986), which is assumed to represent the actual parental melt composition. This figure indicates that trace elements from mineral phases affected by postcrystallization pro-

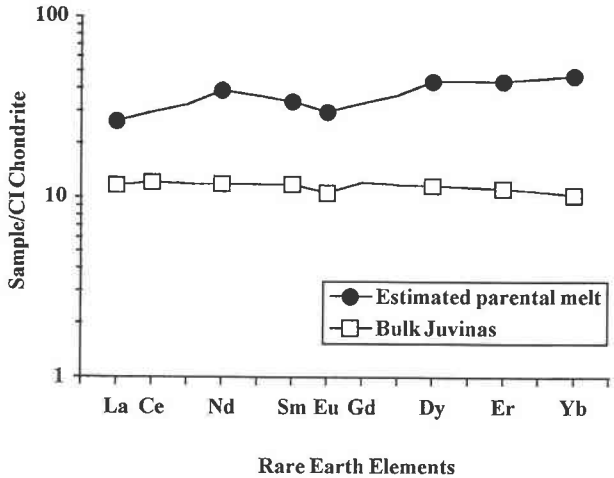

Figure 10. Estimated parental melt compositions for Juvinas calculated from partition coefficients estimated from averaged unequilibrated eucrites (this study). Bulk Juvinas (Shimizu and Masuda 1986) is shown for comparison.

cesses are poor choices for use in interpreting their parental melts and, therefore, their magmatic histories.

Acknowledgments

This work was supported by NASA grants NAGW-3347 (J.J.P.) and NGT-70223 (NASA-GSRP training grant for A.P.) and the Institute of Meteoritics. We sincerely thank K. Yanai and the National Institute of Polar Research for providing all the Antarctic Yamato meteorite samples, and A. Brearley, University of New Mexico, for the Pasamonte and Juvinas samples. We thank M.N. Spilde for his technical assistance with the electron microprobe and major element analyses of Juvinas UNM 210. We also acknowledge G.W. Fowler and G.D. Layne for their technical assistance with the SIMS. SIMS analyses were performed at the UNM/SNL Ion Microprobe Facility, jointly operated by the Institute of Meteoritics of the University of New Mexico and Sandia National Laboratories. We thank Hiroshi Takeda for his helpful discussions and encouragement as well as his insightful review. We also thank Allan Treiman and Jonathan Berg for their helpful reviews. This paper also benefited from reviews by C.K. Shearer, C. Yapp, and A.M. Kudo.

References cited

Anders, E., and Grevesse, N. (1989) Abundances of the elements: Meteoritic and solar. Geochimica et Cosmochimica Acta, 53, 197–214.

Basaltic Volcanism Study Project (1981) Basaltic volcanism on the terrestrial planets, 1286 p. Pergamon, New York.

Bence, A.E., and Papike, J.J. (1972) Pyroxenes as recorders of lunar basalt petrogenesis: Chemical trends due to crystal-liquid interaction. Proceedings of the Lunar Science Conference, 1, 431–469.

Binzel, R.P., and Xu, S. (1993) Chips off asteroid 4 Vesta: Evidence for the parent body of basaltic achondrite meteorites. Science, 260, 186–191.

Boyd, F.R., Jr., and Smith, D. (1971) Compositional zoning in pyroxenes from lunar rock 12021, Oceanus Procellarum. Journal of Petrology, 12, 439–464.

Cameron, M., and Papike, J.J. (1981) Structural and chemical variations in pyroxenes. American Mineralogist, 66, 1–50.

Colson, R.O., McKay, G.A., and Taylor, L.A. (1988) Temperature and composition dependencies of trace element partitioning: Olivine/melt and low-Ca pyroxene/melt. Geochimica et Cosmochimica Acta, 52, 539–553.

Consolmagno, G.J., and Drake, M.J. (1977) Composition and evolution of the eucrite parent body: Evidence from rare earth elements. Geochimica et Cosmochimica Acta, 41, 1271–1282.

Crozaz, G., and McKay, G. (1989) Rare earth elements in Angra dos Reis and Lewis Cliff 86010, two meteorites with similar but distinct magma evolutions. Earth and Planetary Science Letters, 97, 369–381.

Delaney, J.S., Prinz, M., and Takeda, H. (1984) The polymict eucrites. Proceedings of the 15th Lunar and Planetary Science Conference. Journal of Geophysical Research, Supplement, 89, C251–C288.

Drake, M.J. (1979) Geochemical evolution of the eucrite parent body: Possible nature and evolution of asteroid 4 Vesta? In T. Gehrels, Ed., Asteroids, p. 765–782. University of Arizona Press, Tucson.

Floss, C., and Crozaz, G. (1991) Ce anomalies in the LEW 85300 eucrite: Evidence for REE mobilization during Antarctic weathering. Earth and Planetary Science Letters, 107, 13–24.

Fowler, G.W., Shearer, C.K., Papike, J.J., and Layne, G.D. (1995) Diogenites as asteroidal cumulates: Insights from orthopyroxene trace element chemistry. Geochimica et Cosmochimica Acta, 59, 3071–3084.

Graham, A.L., and Yanai, K. (1986) A review of the Yamato-80, -81 and -82 meteorite collections. Memoirs of the National Institute of Polar Research, Special Issue, 41, 167–180.

Grove, T.L. (1982) Use of exsolution lamellae in lunar clinopyroxenes as cooling rate speedometers: An experimental calibration. American Mineralogist, 67, 251–268.

Grove, T.L., and Bartels, K.S. (1992) The relation between diogenite cumulates and eucrite magmas. Proceedings of the Lunar and Planetary Science Conference, 22, 437–445.

Hanowski, N., and Brearley, A.J. (1995) Pyroxene microstructures in the equilibrated eucrite Juvinas. Lunar and Planetary Science, XXVI, 547–548.

Harlow, G.E., and Klimentidis, R. (1980) Clouding of pyroxene and plagioclase in eucrites: Implications for post-crystallization processing. Proceedings of the Lunar and Planetary Science Conference, 11, 1131–1148.

Irving, A.J., and Frey, F.A. (1984) Trace element abundances in megacrysts and the host basalts, constraints on partition coefficients and megacryst genesis. Geochimica et Cosmochimica Acta, 48, 1201–1221.

Mason, B. (1967) The Bununu meteorite, and a discussion of the pyroxene-plagioclase achondrites. Geochimica et Cosmochimica Acta, 31, 107–115.

Mason, B., and Allen, R.O. (1973) Minor and trace elements in augite, hornblende and pyrope megacrysts from Kakanui, New Zealand. New Zealand Journal of Geology and Geophysics, 16, 935–947.

McKay, G.A. (1989) Partitioning of rare earth elements between major silicate minerals and basaltic melts. In Mineralogical Society of America Reviews in Mineralogy, 21, 45–74.

Metzler, K., Bobe, K.-D., Palme, H., Spettel, B., and Stoffler, D. (1994) The Pasamonte polymict eucrite: A reclassification. Lunar and Planetary Science Conference, 25, 901–902.

———(1995) Thermal and impact metamorphism on the HED parent asteroid. Planetary Space Science, 43, 499–525.

Miyamoto, M., Takeda, H., and Yanai, K. (1978) Yamato achondrite polymict breccias. Memoirs of the National Institute of Polar Research, Special Issue, 8, 185–197.

Miyamoto, M., Duke, M.B., and McKay, D.S. (1985) Chemical zoning and homogenization of Pasamonte-type pyroxene and their bearing on thermal metamorphism of a howardite parent body. Proceeding of the 15th Lunar and Planetary Science Conference. Journal of Geophysical Research, Supplement, 90, C629–C635.

Papike, J.J. (1996) Pyroxene as a recorder of cumulate formational processes in asteroids, Moon, Mars, Earth: Reading the record with the ion microprobe. American Mineralogist, 81, 525–544.

Papike, J.J., and Cameron, M. (1976) Crystal chemistry of silicate minerals of geophysical interest. Reviews of Geophysics and Space Physics, 14, 37–80.

Phinney, W.C., Lindstrom, D.J., Mittlefehldt, D.W., and Martinez, R.R. (1993) Post-igneous redistribution of components in eucrites. Lunar and Planetary Science Conference, 24, 1137–1138.

Pun, A., and Papike, J.J. (1995) Ion microprobe investigation of exsolved pyroxenes in cumulate eucrites: Determination of selected trace-element

partition coefficients. Geochimica et Cosmochimica Acta, 59, 2279–2289.

Reid, A.M. (1982) Overview of Antarctic Achondrites. Smithsonian Contributions to the Earth Sciences, 24, 59–64.

Reid, A.M., and Barnard, B.M. (1979) Unequilibrated and equilibrated eucrites. Lunar and Planetary Science Conference, 10, 1019–1021.

Schnetzler, C.C., and Philpotts, J.A. (1969) Genesis of the calcium-rich achondrites in the light of rare earth and barium concentrations. In P.M. Millman, Ed., Meteorite research, p. 206–216. Springer-Verlag, Dordrecht, Holland.

Score, R., King, T.V., Schwarz, A.M., Reid, A.M., and Mason, B. (1982) Description of stony meteorites. Smithsonian Contributions to the Earth Sciences, 24, 19–48.

Shannon, R.D., and Prewitt, C.T. (1970) Revised values of effective ionic radii. Acta Crystallographica, B26, 1046–1048.

Shearer, C.K., Papike, J.J., Simon, S.B., and Shimizu, N. (1989) An ion microprobe study of the intra-crystalline behavior of REE and selected trace-elements in pyroxene from mare basalts with different cooling and crystallization histories. Geochimica et Cosmochimica Acta, 58, 3921–3929.

Shimizu, H., Masuda, A., and Tanaka, T. (1983) Cerium anomaly in REE pattern of Antarctic eucrite. Memoirs of the National Institute of Polar Research, Special Issue, 30, 341–348.

Shimizu, H., and Masuda, A. (1986) REE patterns of eucrites and their genetic implications. Geochimica et Cosmochimica Acta, 50, 2453–2460.

Shimizu, N., Semet, M.P., and Allegre, C.J. (1978) Geochemical applications of quantitative ion-microprobe analysis. Geochimica et Cosmochimica Acta, 42, 1321–1334.

Stolper, E. (1977) Experimental petrology of eucrite meteorites. Geochimica et Cosmochimica Acta, 41, 587–611.

Takeda, H. (1972) Crystallographic studies of coexisting aluminan orthopyroxene and augite of high-pressure origin. Journal of Geophysical Research, 77, 5798–5811.

———(1987) Antarctic Achondrites. In K. Yanai et al., Eds., Sciences of Antarctica, 6, p. 142–179. Kokon-shyoin, Tokyo (in Japanese).

———(1991) Comparisons of Antarctic and non-Antarctic achondrites and possible origin of the differences. Geochimica et Cosmochimica Acta, 55, 35–47.

Takeda, H., Miyamoto, M., and Duke, M.B. (1976) Pasamonte pyroxenes, a eucritic analogue of lunar pyroxenes. Meteoritics, 11, 372–374.

Takeda, H., Miyamoto, M., Duke, M.B., and Ishii, T. (1978a) Crystallization of pyroxenes in lunar KREEP basalt 15386 and meteoritic basalts. Proceedings of the Lunar and Planetary Science Conference, 9, 1157–1171.

Takeda, H., Miyamoto, M., Yanai, K., and Haramura H. (1978b) A preliminary mineralogical examination of the Yamato-74 achondrites. Memoirs of the National Institute of Polar Research, Special Issue, 8, 170–184.

Takeda, H., Miyamoto, M., Ishii, T., Yanai, K., and Matsumoto, Y. (1979) Mineralogical examination of the Yamato-75 achondrites and their layered crust model. Memoirs of the National Institute of Polar Research, Special Issue, 12, 82–108.

Takeda, H., and Yanai, K. (1982) Mineralogical examination of the Yamato-79 achondrites: Polymict eucrites and ureilites. Memoirs of the National Institute of Polar Research, Special Issue, 25, 97–123.

Takeda, H., Mori, H., Yanai, K., and Wooden, J.L. (1982) Three different basalt types in Antarctic polymict eucrites, a view from pyroxene chemical zoning trends. Lunar and Planetary Science Conference, 13, 792–793.

Takeda, H., Wooden, J.L., Mori, H., Delaney, J.S., Prinz, M., and Nyquist, L.E. (1983a) Comparison of Yamato and Victoria Land Polymict eucrites: A view from mineralogical and isotopic studies. Proceedings of the 14th Lunar and Planetary Science Conference. Journal of Geophysical Research, Supplement, 88, B245–B256.

Takeda, H., Mori, H., Delaney, J.S., Prinz, M., Harlow, G.E., and Ishii, T. (1983b) Mineralogical comparison of Antarctic and non-Antarctic HED (howardites-eucrites-diogenites) achondrites. Memoirs of the National Institute of Polar Research, Special Issue, 30, 181–205.

Takeda, H., and Graham, A.L. (1991) Degree of equilibration of eucritic pyroxenes and thermal metamorphism of the earliest planetary crust. Meteoritics, 26, 129–134.

Takeda, H., and Yamaguchi, A. (1991) Recrystallization and shock textures of old and new samples of Juvinas in relation to its thermal history. Meteoritics, 26, 400–401.

Takeda, H., Mori, H., and Bogard, D.D. (1994) Mineralogy and ^{39}Ar-^{40}Ar age of an old pristine basalt: Thermal history of the HED parent body. Earth and Planetary Science Letters, 122, 183–194.

Treiman, A.H. (1995) The perils of partition: Erroneous results from applying $D^{mineral/magma}$ to rocks that equilibrated without magma. Meteoritics, 30, 589.

———(1996) The perils of partition: Difficulties in retrieving magma compositions from chemically equilibrated basaltic meteorites. Geochimica et Cosmochimica Acta, 60, 147–155.

Yamaguchi, A., and Takeda, H. (1992) Mineralogical study of some brecciated Antarctic eucrites. Proceedings of the NIPR Symposium on Antarctic Meteorites, 5, 242–257.

Manuscript received December 20, 1995
Manuscript accepted July 15, 1996